Supporting Information for

Testing Hypotheses About Glacial Dynamics Using a Statistical Model of Paleo-Climate

Robert K. Kaufmann[1], Felix Pretis[2]

[1]Department of Earth and Environment, Boston University, Boston, Massachusetts, USA, 02215

[2]Department of Economics, University of Victoria, Victoria, BC, Canada; and Nuffield College, University of Oxford, Oxford, UK

Corresponding author: Robert K. Kaufmann (Kaufmann@bu.edu)

Contents of this file

Introduction

The supporting information contains text, a figure, and eleven tables that provide details regarding statistical methods and results that are mentioned in the main text. These results concern the use of summer-time insolation at 65^{o}S in the statistical model, uncertainties in the proxy data, the statistical technique that is used to identify simulation errors that are statistically different from zero, and a statistical analysis of the similarity among proxies for ice volume. The tables contain statistical results on these topics and the statistical results reported by Kaufmann and Juselius (2013), results generated when the CVAR model is used to estimate experimental data generated using van der Pol Oscillators, re-estimating the CVAR model reported by Kaufmann and Juselius (2013) which uses a proxy for ice volume that is not orbtially tuned or separates deep water temperature from ice volume.

Text S1. The Choice of summer insolation at 65^{o}S

KJ2013 specifies December insolation at 65^{o}S because it generates the most accurate simulation for *Temp*. As described in KJ2013, the authors estimate twelve CVAR models that specify summer-time insolation at 5^{o} intervals between 60^{o} and 85^{o} north and south and compare the accuracy of in-sample simulations for *Temp* using the test statistic for accuracy (Diebold and Mariano, 1995) As indicated in Supplementary Table 1, the CVAR that uses insolation at 65^{o}S generates the most accurate simulation for Antarctic temperature.

Text S2. Uncertainties in the proxy data

Several of the time series used in the statistical model described in the main text are proxies for physical and/or biological processes. These proxies embody uncertainties that arise from two sources: (1) does the proxy truly represent the physical and/or biological mechanism and (2) does the physical or biological mechanism change as indicated by measurements? These uncertainties are discussed below.

The degree to which measurements of the proxy variable represent the physical or biological process (source strength) depends in part on the way in which the proxy is transported from its source area to the area where the proxy is measured (source transport). Proxies recorded in ice cores are transported to the Antarctic via winds. As such, the source strength that is implied by measurements taken from ice cores can be affected by changes in atmospheric circulation, such as uplift, deposition, and the speed and direction of winds, and processes that affect their atmospheric residence time, such as precipitation. A parallel set of considerations affect the transport of materials from the ocean surface to ocean sediments, such as oceanic currents, re-suspension, and deposition, and biogeochemical processes such as dissolution degradation, and diagenesis (Lee *et al* 2008). For example, Petit and Delmonte (2009) argue that changes in the hydrological cycle and aerosol residence times generate a large portion of the variation in sea salt flux between glacial and interglacial periods. As described below, modeling results and empirical analyses indicate that changes in source transport do not play a major role in the interpretation of source strength for the climate proxies that are included in the CVAR model.

The effect of atmospheric processes on the observed variation in climate proxies over time is investigated using climate models and empirical techniques. Following the former approach, climate models are simulated under glacial and interglacial conditions (e.g. LGM and the Holocene) and changes in the direction and strength of winds and precipitation are recorded. In general, model results suggest that changes in meridonal transport have a relatively small effect on the measured values of proxies (Krinner and Genthon, 1998; Lunt and Valdes, 2001; Reader and McFarlane, 2003; Mahowal *et al* 2006).

A second approach uses empirical measurements to estimate the effect of atmospheric processes on transport strength. For example, Huybrechts (2009) finds that topographic conditions around Antarctica and southern oceans do not change much between glacial and interglacials periods. Shulmeister *et al* (2004) find some evidence that the westerly circulation patterns in the Australian sector of the southern ocean increase slightly during the last glacial maximum. Fisher

et al (2007) find that the ratio of non-sea salt Ca^{+} fluxes in the EDM and the EDC ice cores are relatively constant, which leads them to conclude that transport parameters for dust transport from Patagonia to Antarctica do not change strongly.

Our measure of sea surface temperature is derived from measured values of alkenones from an ocean sediment core. One measure for the uncertainty in SST is given by Kucera *et al* (2005), who find discrepancies among proxies for SST, especially in areas of oceanic upwelling. These discrepancies may be caused by changes in physiological activity. For example, the availability of nutrients and light can affect alkenone measures (Popp *et al.,* 2006; Prahl *et al.,* 2006).

Lee *et al*. (2008) attempt to assess this uncertainty directly by measuring SST along the South west Africa coast, including the Benguela upwelling, and comparing these measurements to estimates of sea surface temperature generated from ocean sediment cores. The results generally are consistent, which implies that oceanic processes between the surface and sediment do not play an important role in estimates of SST derived from alkenones. This reinforces the conclusion generated by Muller *et al* (1997) that species change and nutrient availability does not significantly affect the sedimentary record of alkenones and ultimately temperatures derived therein.

The second source of uncertainty concerns the physical or biological process that the proxy represents. As described below, the source strength of a proxy sometimes is determined by two or more processes, and so it is important to understand the processes represented by the proxy and the degree to which the proxy represents the source strength of the process of interest.

Sea salt sodium (ssNa). At a global scale, sea salt ions, such as ssNa, mostly are generated by bubbles bursting in the open ocean. Wolff *et al* (2003) is the first to propose that ssNa in the Antarctic is derived largely from sea ice surfaces by the formation of frost flowers (Rankin *et al.,* 2000) or the blowing of sea spray (depleted of salt) onto fresh snow which lies on sea ice (Yang *et al*., 2008). Based on these mechanisms, ssNa is used to proxy the area of sea ice in the Indian Ocean sector of the southern ocean around Antarctica (Wolff *et al* 2003, 2006; Fischer *et al* 2007).

Interpreting ssNa as sea ice extent (sie) is supported by two lines of evidence. Maximum concentrations of sea-salt aerosols are found in the Antarctic winter, when sea ice is greatest and this expanded area pushes open water farthest from the Antarctic coast (Sommer *et al.,* 2000; Hara et al., 2004; Weller and Wagenbach, 2007). Consistent with this result, there is a close correlation ($r^2 = 0.78$) between ssNa flux and measured values of sea ice extent in the Indian Ocean and Wedell sea between 1980 and 1999 (Iizuka *et* al., 2008). The geographic origin of ssNa is confirmed by a drop in the correlation coefficient ($r^2 = 0.36$) if ssNa is regressed against sea ice extent in all Antarctic ocean areas (Iizuka *et* al., 208). A second line of evidence for using ssNa to proxy sei is provided by fractionation. Sea salt aerosol is depleted with respect to sulphate, which is inconsistent with an open water source. Conversely, this type of depletion is consistent with sources on the sea ice surface (Jourdain and Legrand, 2002; Jordain *et al.,* 2008).

Despite clear evidence that ssNa can be used to proxy sea ice extent, this proxy has one important limit. Over the last glacial termination, the response of ssNa decreases with increasing sea ice extent, such as during glacial maximums (Rothlisberger *et al*., 2008). This implies that the timing of glacial terminations is not recorded accurately by ssNa (Rothlisbereger *et al*., 2010). Instead, better measures of sea ice extent may be generated by combining ssNa with other proxies, such sea floor diatom abundance (Rothlisbereger *et al*., 2010), but such integrated reconstructions are not available over long periods and so cannot be used to proxy sei in the CVAR estimated over the previous 391Kyr.

Non sea salt sulfate ($nssSO_4$) Using non sea salt sulfate in Antarctic ice cores to proxy biological activity in the southern ocean is established by Cosme *et al* (2005). This biological activity is thought to occur between 58°S and 66°S (Minikin *et* al., 1998; Preunket *et* al., 2007).

Marine biological activity emits dimethylsulphide (DMS), which is converted to methanesulphonate (MSA) and sulfate in the atmosphere. For the Antarctic, biological activity is the only source for MSA, but because its presence declines after being deposited (Weller *et* al.,

2004), MSA is not used to proxy biological activity. Conversely, sulfate is fully preserved in the snowpack following deposition (Silvente and Legrand, 1993) and therefore has the potential to proxy for marine biological activity over long periods.

Using non sea salt sulfate to proxy biological activity contains several uncertainties. Unlike MSA, sulfate in Antarctic ice cores has several sources, such as terrestrial dust and volcanism (Wolff *et al* 2006). Although volcanic sources contribute less than 10 percent of sulfates that are transported to Antarctica during background periods (Cosme *et al*., 2005), volcanic sources could dominate for one to three years after an eruption. But such sources account for less than 6 percent of the Holocene sulfate budget (Wolff *et al*., 2006).

Also, there is uncertainty regarding the correlation between sulfate and biological activity. The proportion of DMS that is converted to sulfate (as opposed to MSA) is not known precisely and so changes in 'yield' can alter the correlation between the DMS emitted by biological activity and the sulfate deposited in ice cores. Despite this potential source of decoupling, sulfate always is the main product from the oxidation of DMS (Legrand and Pasteur, 1998).

Iron (Fe) *and non sea salt calcium (Ca)* originate from terrestrial material. This terrestrial material is thought to originate largely from Patagonia in South America. Wolff *et al* (2006) argue that changes measured in the Dome C core represent changes in source strength. Changes in source strength have several possible causes (Wolff *et al* 2006). They include (1) changes in local climate and/or vegetative cover, (2) changes in the extent of glaciers, and (3) changes in sea level that increase/decrease the source area. Of these possible causes, Wolff *et al* (2006) conclude that *Ca* reflects changes in wind strength and aridity, with a possible role by glaciers.

Given the similarity in source area and source strength both *Ca* and *Fe* are used to represent the iron fertilization effect in statistical models (e.g. Rothlisberger *et al*., 2004*;* Kaufmann *et al.,* 2010). In our sample period, the time series for *Fe* and *Ca* are highly correlated ($r^2 = 0.75$—see sections III and V on the limits of using r^2 to measure the correlation between nonstationary variables). Our results indicate that using *Fe* to measure the iron fertilization effect generates

'better' statistical results than using *Ca*. For example, replacing *Fe* with *Ca* in *CR #6* generates a positive relation between SO_4 and *Ca*. But if we add *Ca* to the sixth cointegrating relationship and retain *Fe*, there is still a positive relation between *Fe* and SO_4, whereas the relation between *Ca* and SO_4 is negative. This would suggest that in a 'head-to-head' comparison, *Fe* is a better proxy for the iron fertilization effect than *Ca*. This result is consistent with the arguments made by Wolff *et al* (2006) that *Fe* is preferred to *Ca* with regards to discussion of iron fertilization.

Sea Surface temperature (*SST*) is proxied using alkenones from a core drilled at site PS2489-2/ODP1090 in the subantatarctic Atlantic. Alkenones are organic compounds that are produced by phytoplankton in the class Prymnesiophyceae, such as coccolithophores. Alkenones resist decay and therefore are stable over long periods, which makes them an ideal proxy.

Alkenones are used to measure sea surface temperature because the organisms that produce them live within the ocean surface layer and the degree to which alkenones are saturated depends on the temperature at which they are produced. Specifically, high temperatures favor the production of di-unsaturated molecules relative to tri-unsaturated molecules (Prahl and Wakeham, 1987). To measure these differences, Prahl and Wakeham, (1987) describe an alkenone unsaturation index:

$$U_{37}^{K\prime} = \frac{C_{37:2}}{C_{37:2}+C_{37:3}} \qquad \text{(Supplementary Equation 1)}$$

in which $C_{37:2}$and $C_{37:3}$ are diunstaurated and triunsaturated C_{37} alkenones. This ratio is used to calculate temperature (T) as follows:

$$T = \frac{U_{37}^{K\prime}-0.039}{0.034} \qquad \text{(Supplementary Equation 2)}$$

which also is generated by Prahl and Wakeham (1987).

Empirical analyses validate the conversion to temperature that is given by equation S.2. Muller *et al.*, (1998) examine the relation between observed sea surface temperature and that calculated using equation S.2 for tropical to subtropical (27^o) sites. Their results strongly validate the use of alkenones to proxy sea surface temperature (0 to 10 meters).

The power of alkenones to proxy sea surface temperature is confirmed by Lee *et al*., (2008), who analyze the relation between sea surface temperature and two proxies, alkenones and glycerol dibiphytanyl glycerol tetraether (GDGT). They find that sea surface temperatures generated from alkenones "are in general consistent with in situ temperatures, even in the dynamic upwelling areas." This performance is superior to the accuracy of temperature estimates generated from GDGT. As such, alkenones seem a reasonable proxy for SST.

Text S3. Testing whether simulation errors are statistically different than values from the proxy record

Statistical tests to determine whether simulation errors are statistically different than values from the proxy record are complicated by autocorrelation of the errors, which is caused by the use of a dynamic simulation for the simulated time series and additionally through potential mis-specification (Hendry and Richard, 1982).

To control for the autocorrelation in the errors, each simulation error is modelled using a dynamic autoregressive model of order two (to match the dynamics of the original CVAR)[1] while selecting over a full set of step-break functions using SIS in the R-package *gets* (Pretis *et al*., 2018). Shifts in each variable's simulation error are selected at a significance level of $p_\alpha = 1/T$ (where T is the sample length of each simulation error), which implies an expected false positive rate (gauge) of one shift per simulation error. The final model for each simulation error is then given by k_i breakpoints for each simulation error ϵ_i where i refers to the variable under consideration (e.g. Temperatures, or CO_2) in (S.3):

$$\epsilon_{i,t} = \sum_{j=1}^{k_i} \mu_j + \rho_1 \epsilon_{i,t-1} + \rho_2 \epsilon_{i,t-2} + u_{i,t} \text{ (Supplementary Equation 3)}$$

[1] The overall results are largely unaffected if selection takes place over the autoregressive coefficients instead of using a fixed lag length.

To test whether the simulation errors are different from zero, we construct the time-varying long-run mean of the error (Hendry, 1994) up to each breakpoint determined by SIS for *j=1,2…,k-1,k* as:

$$\hat{\varphi}_{\varepsilon,k} = \frac{\sum_{j=1}^{k} \hat{\mu}_t}{1-\sum_{l}^{n} \hat{\rho}_l} == \qquad \text{(Supplementary Equation 4)}$$

in which $\hat{\mu}_j$ is the regression intercept as given by the regimes determined using SIS while $\hat{\rho}_l$ denote the estimated autoregressive coefficients up to a maximum lag length of n=2. The long-run mean describes the expectation of the simulation error – in other words the long-run value towards which the error converges if it is not disturbed by shocks.

To determine whether a model error for variable *i* in time step *t* is systematically different from zero and thus, whether the simulated value is biased, we construct an approximate 95% confidence interval around this time-varying long-run mean using its estimated variance [2] To account for potential under-estimation of the variance in indicator saturation models, the estimated variance is corrected for consistency and efficiency using factors developed by Johansen and Nielsen (2016). To differentiate between one-time and persistent failures, outliers in simulation errors are defined as statistically significant events for one time step, while persisting errors (or systematic biases) describe periods when the bias persists for two or more time-steps. Note that the outliers in dynamic (autoregressive) models of simulation errors that are detected by the methodology correspond to innovational outliers that propagate through the system (e.g. Nielsen 2004) – a single outlier can be indicative of a longer period of subsequent simulation failure.

We illustrate the process of identifying persisting errors using the simulation error for CO_2. The top panel of Figure S1 shows the value for CO_2 simulated by the model (blue line) and the value from the proxy record (black line). The simulation error, which is the difference between the black and blue lines is given in the lower panel. This panel also shows the time-varying long-run

[2] Testing whether the time-varying intercept equals zero (μ_j=0) yields close to identical results to testing on the long-run mean ($\phi_{\epsilon,k} = 0$), as μ_j=0 implies $\phi_{\epsilon,k} = 0$ in equation (5).

mean (blue line) and its approximate 95% confidence interval (blue-dashed lines). There is no persisting error if the dashed blue lines include zero (the red line) as they do until about -428 kyr ago. At this time, there Note that the significant upward shift in the form of an outlier of the simulation error around -428ka increases. But so too does the 95% confidence intervals, such that we cannot reject a zero long-run mean during the time period that follows. As such, there is no persisting error during this period.

Text S4. Cointegrating relations among proxies for ice volume

We investigate the relation among the three proxies for *Ice* by testing whether they cointegrate using the Engle and Granger (1987) two step procedure. First, we use OLS to estimate the relation between proxies by estimating the following regression:

$Ice_{i,t} = \alpha + \beta Ice_{j,t} + \mu_t$ (Supplementary Equation 5)

In which *Ice* is the proxy for ice volume compiled by source i or j, α and β are regression coefficients, and μ is the regression residual.

In the second step, the regression residual μ is tested for a stochastic trend using a test developed by Eliot *et al* (date), which has the null hypothesis that the series has a stochastic trend. The results reject the null hypothesis which indicate that the proxies for ice volume cointegrate with one another (Supplementary Table 11). As such, the three proxies for ice volume share the same long-term pattern, which implies that they measure the same glacial cycles.

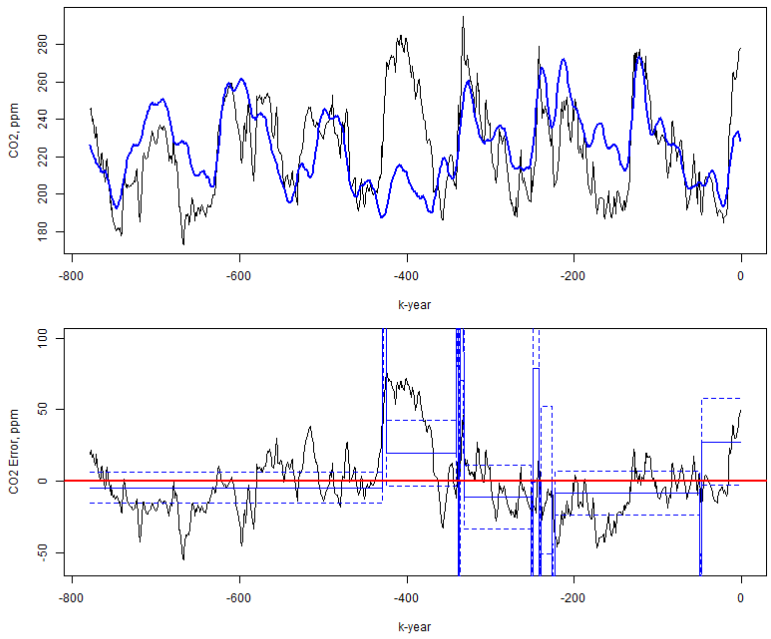

Figure S1. Endogenously simulated CO_2 and its simulation error relative to observations. Top panel shows observed CO_2 (black) from -800k years until present together with simulated CO_2 (blue) using the CVAR model. Lower panel shows CO_2 Model error (black, difference between observed and simulated in top panel) together with its time-varying long-run mean (blue) where regimes are determined using SIS. An approximate 95% confidence interval for the long-run mean is given by the blue-dashed lines. Note that the significant upward shift in the form of an outlier of the simulation error around -428ka increases the level of the long-run mean relative to its prior value, however, the increased uncertainty (as evidenced by the wider confidence interval) implies that we cannot reject a zero long-run mean during the time period that follows.

	N60	S60	N65	S65	N70	S70	N75	S75	N80	S80	N85	S85	Wins	Losses
N60	--	-1.42	-2.03	1.92	-0.71	0.91	0.61	-0.71	1.82	-1.11	2.94	0.51	1	1
S60	--	--	-0.71	3.04	0.81	1.72	1.92	2.13	2.63	0.00	2.13	2.53	0	5
N65	--	--	--	3.95	0.91	3.34	4.46	1.11	3.44	0.00	2.23	2.33	0	7
S65	--	--	--	--	-2.73	-3.24	-2.33	-2.23	-2.33	-2.53	-1.72	-3.85	9	0
N70	--	--	--	--	--	2.13	2.73	1.01	1.62	-2.53	1.32	1.72	1	3
S70	--	--	--	--	--	--	1.22	-1.01	0.81	-2.84	-0.91	-1.72	3	1
N75	--	--	--	--	--	--	--	-2.33	2.84	-3.14	1.52	-1.42	4	2
S75	--	--	--	--	--	--	--	--	2.94	-2.43	2.33	0.41	2	4
N80	--	--	--	--	--	--	--	--	--	-2.03	0.20	-3.44	6	1
S80	--	--	--	--	--	--	--	--	--	--	2.53	1.52	0	7
N85	--	--	--	--	--	--	--	--	--	--	--	-3.14	6	0
S85	--	--	--	--	--	--	--	--	--	--	--	--	2	3

Table S1 Accuracy of simulations generated by CVAR models estimated using summer insolation at various latitudes. Values represent the test statistic developed by Diebold and Mariano (1995). Positive values (greater than about 2.0) indicate the simulation generated by insolation at the latitude identified at the start of the row is more accurate than the simulation at the latitude identified at the top of the column.

	Temp	***Co2***	***CH4***	***Ice***	***Fe***	***Na***	***SO4***	***Ca***	***Level***	***SST***	***Ecc***	***Obl***	***Prec***	***Sum***	***K***
CR#1	1.00**	-0.83**	--	--	--	--	--	--	--	--	--	--	--	--	--
CR#2		--	1.00**	0.89**	--	--	--	--	--	--	0.18**	--	--	--	--
CR#3	--	0.97**	--	1.00**	--	--	--	--	--	--	0.10**	--	--	--	--
CR#4	--	--	--	--	1.00**	--	--	-0.16**	0.85**	--	--	2.02**	-0.08*	--	--
CR#5	--	--	--	--	0.25**	1.00**	--	--	--	1.00**	--	--	--	0.24*	--
CR#6	--	--	--	--	-0.71**	--	1.00**	--	--	-	--	--	--	--	--
CR#7	--	--	--	--	--	--	--	1.00**	0.71**	--	0.25**	--	--	--	--
CR#8	--	2.5**	--	2.06**	-	--	--	--	1.00**	-1.29**	--	--	--	--	--
CR#9	--	1.00**	--	--	--	2.02**	0.43**	--	--	0.77**	--	--	--	--	--
CR#10	--	--	--	1.00**	--	--	--	--	--	--	0.76**	-4.46**	--	-2.88**	--

Test statistics are statistically significantly different from zero at the: **1%, *5%, +10% level

Table S2 Elements of the β matrix in the CVAR model reported by Kaufmann and Juselius (2013).

	CR#1	CR#	CR#3	CR#4	CR#5	CR#6	CR#7	CR#8	CR#9	CR#10
Temp	-0.50**	-0.14**	-0.04	0.05	0.14	0.13**	-0.06+	-0.101	-0.38**	0.07**
CO2	0.17**	-.11**	-0.21**	0.01	0.18*	0.05+	-.09**	0.16*	-0.23*	0.04*
CH4	0.23*	-0.50**	0.15	-0.07	0.18	0.04	-0.05	0.20	-0.243	0.03
Ice	-0.09+	-0.01	-0.11+	-0.04	-0.08	-0.04	0.03	-0.08	0.09	-0.04*
Fe	0.12+	0.10*	-0.60**	-0.45**	0.64**	0.13**	0.09*	0.80**	-0.62**	-0.10**
Na	-0.08+	0.05*	-0.01	0.03	0.12+	0.07*	-0.03	0.04	-0.33**	-0.03*
SO4	0.07	0.06	-0.27*	-0.23**	0.24*	-0.16**	0.02	0.30*	-0.25+	-0.09**
Ca	0.10*	0.03	-0.26**	-0.04	0.33**	0.08*	-0.17**	0.35**	-0.35**	0.001
Level	-0.09*	0.02	0.18**	0.06*	-0.20**	-0.02	-0.04+	-0.30**	0.16*	0.01
SST	0.03	-0.07**	0.01	0.04	-0.18*	-0.01	0.03	-0.02	0.14+	0.02*

Test statistics are statistically significantly different from zero at the: **1%, *5%, +10% level

Table S3 Elements of the α matrix in the CVAR model described by Kaufmann and Juselius (2013).

	Π (15)	Γ (10)	A_0 (4)	A_1 (4)	Total
Temp	7	4	2	2	15
CO2	7	3	1	1	12
CH4	4	0	2	1	7
Ice	4	2	1	1	8
Fe	8	1	2	2	13
Na	5	1	2	2	10
SO4	6	1	1	1	9
Ca	7	2	0	0	9
Sea Level	7	2	1	1	11
SST	3	1	3	2	9

Numbers in parenthesis refers to the number of columns in the matrix, which corresponds to the number of coefficients estimated.

Table S4 Variables per equation in CVAR reported by Kaufmann and Juselius (2013). Values represent the number of variables that are statistically different from zero ($p < 0.05$) in each equation

	I	T	F	Constant
CR#1	0.912	0.596	0.003	-0.053
CR#2	0.813	-0.979	0.001	-0.009

Table S5 Elements of the β matrix in the CVAR estimated from the experimental data generated by the van der Pol Oscillators. No standard errors are available because no overidentifying restrictions are imposed.

	CR #1	CR #2
$\Delta \boldsymbol{I}$	-0.035***	0.038***
$\Delta \boldsymbol{T}$	0.028***	0.026***

Table S6 Elements of the α matrix in the CVAR estimated from the experimental data generated by the van der Pol Oscillators.

	Temp	***Co2***	***CH4***	***Ice***	***Fe***	***Na***	***SO4***	***Ca***	***Level***	***SST***	***Ecc***	***Obl***	***Prec***	***Sum***	***K***
CR#1	-0.90***	1.00	0.00	--	--	--	--	--	--	--	--	--	--	--	--
CR#2	--	--	-0.27***	1.00	--	--	--	--	--	--	0.37***	--	--	--	--
CR#3	--	-0.31***	0.00	1.00	--	--	--	--	--	--	0.39***	--	--	--	--
CR#4	--	--	0.00	--	0.06	--	--	0.71***	1.00	--	--	0.77*	-0.01*	--	--
CR#5	--	--	0.00	--	0.06	1.00	--	--	--	0.79***	--	--	--	-0.78**	--
CR#6	--	--	0.00	--	-0.71**	--	1.00	--	--	--	--	--	--	--	--
CR#7	--	--	0.00	--	--	--	--	1.00	-0.69***	--	0.62***	--	--	--	--
CR#8	--	-0.69***	0.00	-0.41***	--	--	--	--	-0.97***	1.00	--	--	--	--	--
CR#9	--	1.00	0.00	--	--	0.49***	0.07***	--	--	-0.31***	--	--	--	--	--
CR#10	--	--	0.00	1.00	--	--	--	--	--	--	0.32***	0.21*	--	0.31	--

Test statistics are statistically significantly different from zero at the: **1%, *5%, +10% level

Table S7 Elements of the β matrix in the CVAR model estimated using the proxy for ice volume compiled by Huybers (personal communication) $\chi^2(26) = 26.3, p > 0.44)$

	CR#1	CR#	CR#3	CR#4	CR#5	CR#6	CR#7	CR#8	CR#9	CR#10
Temp	0.52***	0.48***	2.38+	0.60+	-0.76*	-0.03	-0.49+	0.98	1.08	-2.44*
CO2	-0.25***	0.35***	0.92	0.26	-0.34	-0.06	-0.27	0.46	0.61	-1.12
CH4	-0.28*	1.87***	-3.41	-0.62	0.59	0.07	0.42	-0.90	-1.29	1.14
Ice	-0.02*	-0.01	-0.36+	-0.11*	0.12+	0.01+	0.09 *	-0.17+	-0.22+	0.26
Fe	-0.10	-0.39*	-13.41***	-3.66***	4.06***	0.60***	2.75***	-5.75***	-8.24***	11.45***
Na	0.08	-0.19 *	0.85	0.25	-0.39	-0.02	-0.21	0.40	0.36	-0.52
SO4	-0.10	-0.22	-7.28***	-2.01***	2.15***	0.12+	1.49***	-3.07***	-4.40***	6.21***
Ca	-0.07	-0.13	-0.09	-0.13	0.07	0.02	-0.08	-0.08	-0.19	0.23
Level	0.08+	-0.03	1.34+	0.28	-0.42+	-0.04	-0.24	0.58 +	0.79+	-1.10+
SST	-0.03	0.27*	0.72	0.18	-0.27	-0.01	-0.13	0.24	0.49	-0.89

Test statistics are statistically significantly different from zero at the: **1%, *5%, +10% level

Table S8 Elements of the α matrix in the cointegrating relations for the CVAR model estimated using the proxy for ice volume compiled by Huybers (personal communication).

	Temp	*Co2*	*CH4*	*Ice*	*Fe*	*Na*	*SO4*	*Ca*	*Level*	*SST*	*Ecc*	*Obl*	*Prec*	*Sum*	*K*
CR#1	1	-0.91***	--	--	--	--	--	--	--	--	--	--	--	--	--
CR#2	--	--	1	1.05***	--	--	--	--	--	--	0.16*	--	--	--	--
CR#3	--	0.91***	--	1	--	--	--	--	--	--	0.06***	--	--	--	--
CR#4	--	--	--	--	1	--	--	0.14**	1.23***	--	--	1.04***	-0.06+	--	--
CR#5	--	--	--	--	0.328***	0.79***	--	--	--	1	--	--	--	0.22**	--
CR#6	--	--	--	--	-0.83***	--	1	--	--	--	--	--	--	--	--
CR#7	--	--	--	--	--	--	--	1	0.55***	--	0.27***	--	--	--	--
CR#8	--	4.53***	--	4.054**	--	--	--	--	1	-1.42***	--	--	--	--	--
CR#9	--	1	--	--	--	1.96***	0.57***	--	--	1.14***	--	--	--	--	--
CR#10	--	--	--	1	--	--	--	--	--	--	0.46***	-1.88**	--	-1.28*	--

Test statistics are statistically significantly different from zero at the: **1%, *5%, +10% level

Table S9 Elements of the β matrix in the CVAR model in the CVAR model estimated using the proxy for ice volume compiled by Elderfield *et al*., (2012) Overidentified restriction are not rejected $\chi^2(26) = 14.2, p > 0.97$)

	CR#1	CR#	CR#3	CR#4	CR#5	CR#6	CR#7	CR#8	CR#9	CR#10
Temp	-0.51^{***}	-0.11^{*}	0.36	0.10^{+}	0.04	0.14^{*}	-0.08^{+}	-0.11^{*}	-0.13^{+}	0.13^{***}
CO2	0.16^{**}	-0.09^{**}	-0.23	0.02	0.15	0.06	-0.10^{*}	0.04	-0.08	0.08^{***}
CH4	0.21^{*}	-0.48^{***}	-0.19	-0.10	0.41	0.10	-0.03	0.14	-0.19	0.09^{*}
Ice	-0.14^{*}	0.00	0.19	0.08^{+}	-0.29^{*}	-0.03	-0.04	-0.11^{*}	0.11^{+}	-0.01
Fe	0.12^{+}	0.10^{*}	-2.43^{***}	-0.60^{***}	1.55^{***}	0.35^{****}	0.24^{***}	0.61^{***}	-0.61^{***}	-0.08^{**}
Na	-0.08^{+}	0.04^{+}	0.05	0.04	0.17	0.10^{*}	-0.04	-0.01	-0.18^{**}	-0.07^{**}
SO4	0.05	0.07^{+}	-1.15^{**}	-0.33^{***}	0.74^{**}	-0.03	0.10^{+}	0.28^{***}	-0.30^{**}	-0.11^{***}
Ca	0.08^{+}	0.03	-0.63^{**}	-0.07^{+}	0.43^{**}	0.11^{*}	-0.15^{***}	0.15^{**}	-0.19^{**}	0.02
Level	-0.09^{*}	0.02	0.74^{***}	0.10^{**}	-0.43^{***}	-0.07^{*}	-0.06^{*}	-0.19^{***}	0.16^{**}	0.00
SST	0.03	-0.06^{*}	0.22	0.07^{*}	-0.30^{*}	-0.04	-0.01	-0.05	0.10^{*}	0.04^{*}

Test statistics are statistically significantly different from zero at the: **1%, *5%, +10% level

Table S10 Elements of the α matrix in the cointegrating relations in the CVAR model estimated using the proxy for ice volume compiled by Elderfield *et al*., (2012).

$Ice_{i,t}$	$Ice_{j,t}$	DFGLS
Lisiecki and Raymo (2005).	Elderfield *et* al., 2012	-8.86^{**}
Lisiecki and Raymo (2005)	Huybers (personal communication	-4.31^{**}
Elderfield *et* al., 2012	Huybers (personal communication	-3.98^{**}

Test statistics are statistically significantly different from zero at the: **1%, *5%, +10% level

Table S11 Tests of cointegration between proxies for ice volume. The GLS estimate of the Dickey-Fuller statistic is used to test for cointegration (Supplementary Equation 5)

Literature Cited

Basile, I., F.E. Grousset, M. Revel, J.R. Petit, P.E. Biscaye, N.I. Barkov, NI, 1997, Patagonian origin of glacial dust deposited in East Antarctica (Vostok and Dome C) during glacial stages 2, 4 and 6, *Earth and Planetary Science Letters* 146(3-4): 573-589 DOI: 10.1016/S0012-821X(96)00255-5

Bigler, M. R. Rothlisberger, F. Lambert, E.W. Wolff, E. Castellano, R. Udisti, T.F. Stocker, H. Fischer, 2010, Atmospheric decadal variability from high-resolution Dome C ice core records of aerosol constituents beyond the last interglacial, *Quaternary Science Reviews* 29:324-337.

Cosme, E. F. Hourdin, C. Genthon, and P. Martinerie, 2005, Origin of dimethylsulfide, non-sea-sal sulfate, and methanesulfonic acid in eastern Antartica, *J. Geophys. Res.* 110 (D03302), doi:10.1029/2004JD004881.

Diebold, F.X., and Mariano, R.S.: Comparing predictive accuracy. *J. of Bus. & Econ Stat.*, **13**, 253-263 (1995).

Elderfield, H., Ferretti P., Crowhurst, S., McCave, I.N., Hodell, D., and Piotrowski, A.M., Evolution of ocean temperature and ice volumne through the mid-Pleisocene climate transition, *Science* 337(6096):704-709 (2012).

Engle, R.E. and Granger, C.W.J. (1987) 'Cointegration and error-correction: representation, estimation, and testing' *Econometrica* **55**, 251-276

Fischer, H. F. Fundel, U. Ruth, B. Twarloh, A. Wegner, R. Udisti, S. Becagli, E. Castellano, A. Morganti, M. Siveri, E. Wolff, G. Littot, R. Rothlisberger, R. Mulvaney, M. A. Hutterli, P. Kaufmann, U. Federer, F. Lambert, M. Bigler, M. Hansson, U. Jonsell, M. Angelis, C. Boutron, M. Siggard-Andersen, J. P. Steffensen, C. Barbante, V. Gaspri, P. Gabrielli, D. Wagenbach, 2007, Reconstruction of millennial changes in dust emission, transport and regional sea ice coverage using the deep EPICA ice cores from the Atlantic and Indian ocean sector of Antarctica, *Earth and Planetary Science Letters* 260:340-354.

Hara, K. K. Osada, M. Kido, M. Hayashi, K. Matsunaga, Y. Iwasaka, T. Yamanouchi, G. Hashida, and T. Fukatsu, 2004, Chemistry of sea-salt particles and inorganic halogen species in Antarctis regions: compositional differences between coastal and insland stations *J. Geophys. Res*. 109, doi:10.1029/2004JD004713.

Hendry, D. and Juselius, K. 2000, Explaining cointegration analysis: Part 1, *Energy Journal*, 21, 1–4.

Hendry, D. and Richard, J.F.: On the Formulation of Empirical Models in Dynamic Econometrics, Journal of Econometrics, 20(1), 3-33, 1982

Huybrechts, P. 2009, Cryosphere In: Gornitz, V. (ed.) Encyclopedia of Paleoclimatology and Ancient Environments Springer Dordrecht, The Netherlands, P. 221-225.

Iizuka, Y. T. Honodoh, and Y. Fuji, 2008, Antacrtic sea ice extent during the Holocene reconstructed from inland ice core evidence, *J. Geophys. Res.* 113 (D15114) doi:10.1029/2007/JD009326).

Johansen, S., & Nielsen, B. (2016). Asymptotic theory of outlier detection algorithms for linear time series regression models. *Scandinavian Journal of Statistics*, *43*(2), 321-348.

Jordain, B. and Legrand, M. 2002, Year-round records of bulk and size-segregated aerosol composition and HCL and HNO3 levels in the Dumont d'Urville (coastal Antarctica) atmosphere: implications for sea-salt aerosol fractionation in the winter and summer, *J. Geophys. Res*. 107(D22). 4645. Doi:10.1029/2002JD0002471.

Jordain, B. S. Preunker, O. Cerri, H. Casterunet, R. Udista, M.R. Legrand, 2008, Year round record of size-segregated aerosol composition in central Antartica (Concordia station) implications for the degree of fractionation of sea salt particles *J. Geophys. Res.* 113 (D14308) doi:10.1029/2007/JD009584.

Kaufmann, P. F. Fundel, H. Fischer, M. Bigler, U. Ruth, R. Udisti, M. Hansson, M. Angelis, C. Barbante, E.W. Wolff, M. Hutterli, D. Wagenbach, 2010, Ammonium and non-sea salt sulfate in the EPICA ice cores as indicator of biological activity in the Southern Ocean, *Quaternary Science Reviews* 29:313-323.

Krinner, G. and C. Genthon, 1998. GCM simulation of the last glacial maximum surface climate of Greenland and Antartica, *Clim. Dyn.* 14:741-758.

Kucera, M, A. Roselle-Mele, R. Schneider, C.Waelbroeck, and M. Weinelt, 2005, Multiproxy approach for the reconstruction of the glacial ocean surface (MARGO) *Quaternary Science Review*, 24:813-819.

Lee, K.E. J.H. Kim, I. Wilke, P. Helmke, S. Schouten, 2008, A study of the alkenone, TEX_{86} and planktonic foraminifera in the Benguela upwelling system: implications for past sea surface temperature estimates, *Geochemistry, Geophysics, Geosystems,* 9(10), Q10019, doi:10.1029/2008GC002056.

Legrand, M . and E.C. Pasteur, 1998, Methane sulfonic acid to non-sea-salt sulfate ratio in coastal Antarctic aerosol and surface snow, *J. of Geophys. Res.* 103: 1099-11006.

Lisiecki, L. E. and Raymo, M. E. 2005, A Pliocene-Pleistocene stack of 57 globally distributed benthic $\delta^{18}O$ records, *Paleoceanography*, 20, 1–17.

Lunt, D.J. and P.J. Valdes, 2001, Dust transport to Dome C, Antarctica, at the last glacial maximum and present day, *Geophysical Research Letters,* 28(2):295-298,

Mahowal, N. K. Kohfeld, M. Hansson, Y. Balkanski, S.P. Harrison, I.C. Prentice, M. Schulz, and H. Rodhe, 1999, dust sources and deposition during the last glacial maximum and current climate a comparison of model results with paleodata from ice cores and marine sediments *J. Geophys. Res*. 104:15895-15916.

Minikin, A. M. Legrand, J. Hall, D. Wagenbach, C. Kleefel, E.W. Wolff, E. Pasteur, and F. Ducroz, 1998, sulfur containing species (sulfate and methanesulfonate) in coastal Antarctic aerosol and precipitation, *J. Geophys. Res*. 103:10975-10990.

Muller, P.J. G. Kirst, G. Ruhland, I. von Storch, and A. Rosell-Mele, 1998, Calibration of the alkenone paleotemperature index U-37(K ') based on core-tops from the eastern South Atlantic and the global ocean (60 degrees N-60 degrees S), *Geochimica et Cosmochimica Acta* 62(10): 1757-1772, DOI: 10.1016/S0016-7037(98)00097-0.

Nielsen, H. B. 2004. Cointegration analysis in the presence of outliers. *The Econometrics Journal*, *7*(1), 249-271.

Petite, J.R. and B. Delmonte, 2009, A model for large glacial-interglacial climate-induced changes in dust and sea salt concentrations in deep ice cores (central Antarctica): paleoclimatic implications and prospects for refining ice core chronologies, *Tellus* doi:10:1111/j.600-0889.2009.00437x.

Popp, B.N. F.G. Prahl, J. Wallsgrove, and J. Tamimoto, 2006, Seasonal patterns in alkenone production in the subtropical oligotrophic North Pacific, *Paleoceanography* 21 PA1004, doi10.1029/2005PA001165.

Prahl, F.G. and S.G. Wakeham, 1987, Calibration of unsaturation patterns in long-chain ketone compositions for palaeotemperature assessment, *Nature* 330:367-369, doi:10.1038/330367a0

Prahl, FG., A.C. Mix, and M.A. Sparrow, 2006, Alkenone paleothermometry: biological lessons from marine sediment records off western South America *Geochim. Cosmochin. Acta. 70:* 101-117.

Pretis, F., Reade, J., & Sucarrat, G.: Automated General-to-Specific (GETS) regression modeling and indicator saturation methods for the detection of outliers and structural breaks. Journal of Statistical Software, 86(3), 2018.

Preunkert, S., M. Legrand, B. Jourdain, C. Moulin, S. Belviso, N. Kasamatsu, M. Fukuchi, T. Hirawake, 2007, Interannual variability of dimethylsulfide in air and seawater and its atmospheric oxidation by-products (methanesulfonate and sulfate) at Dumont d'Urville, coastal Antarctica (1999-2003), *J. Geophy. Res.* 112: D6 (D06306) doi: 10.1029/2006JD007585

Rankin, A.M., V. Auld, E.W. Wolff, 2000. Frost flowers as a source of fractionated sea salt aerosol in polar regions, *Geophsyiscal Research Letters* 27(21):3469-3472.

Reader, M.C. and N. McFarlane, 2003, Sea salt aerosol distribution during the last glacial maximum and its implications for mineral dust, *J. Geophys.* Res 108. Doi:10.1029/2002JD002063.

Roethlisberger, R., M. Mudelsee, M. Bigler, M. de Angelis, H. Fischer, M. Hansson, F. Lambert, V. Masson-Delmotte, L. Sime, R. Udisti, E.W. Wolff, 2008, 2008, The Southern Hemisphere at glacial terminations: insights from the Dome C ice core, *Climate of the Past* 4(4): 345-356.

Rothlisberger, R. X. Crosta, N.J. Abram, L. Armand, E.W. Wolff, 2010, Potential and limitations of marine and ice ore sea ice proxies: an example from the Indian Ocean sector, *Quaternary Science Reviews* 29:296-302.

Schulmeister, J. I. Goodwin, J. Renwick, K. Harle, L. Armand, M.S. McGlone, E. Cook, J. Dodson, PP. Hesse, P. Mayewski, M. Curran, 2004. The Southern Hemisphere westerlies in the Australian sector over the last glacial cycle: a synthesis. *Quaternary International* 118-119:23-53.

Shakun, J.D. P.U. Clark, F. He, S.A. Marcott, A.C. Mix, Z. Liu, B. Otto-Bliesner, A. Schmittner, E. Bard, Global warming preceeded by increasing carbon dioxide concentrations during the last deglaciation, 2012, *Nature 484:49-54.*

Shine K. P. R. G., D. J. Derwent, D. J. Wuebbles, and J.J. Mocrette, Radiative forcing of climate, in J. T. Houghton, G. J. Jenkins, and J. J. Ephramus (eds.)*Climate Change: The IPCC Scientific Assessment*, Cambridge University Press, pp. 47-68, 1991.

Sommerm S., D. Wagenbach, R. Mulvaney, H. Fischer, 2000, Glaciochemical study covering the past 2 kyr on three ice cores from Dronnin Maud Land, Antarctica 2. Seasonally resolved chemical records, *J. Geophys. Res.* 105, 29423-29433.

Weller, R., F. Traufetter, H. Fischer, H. H. Oerter, C. Piel, H, Miller, H. 2004. Postdepositional losses of methane sulfonate, nitrate, and chloride at the European Project for Ice Coring in Antarctica deep-drilling site in Dronning Maud Land, Antarctica, *J. Geophys. Res.* 109:D7 (D07301) doi: 10.1029/2003JD004189

Wolff, E.W. A.M. Rankin, R. Rothlisberger, 2003, An ice core indicator of Antactic sea ice production? *Geophys. Res. Lett.* 30 doi:10.1029/2003GLO18454.

Yule, G. 1929 *An Introduction to the Theory of Statistics*, C. Griffin and Co., London.